5286–5296 *Nucleic Acids Research, 2018, Vol. 46, No. 10* *Published online 5 January 2018*
doi: 10.1093/nar/gkx1309

Snapshots of a molecular swivel in action

Caitlin S. Trejo[1], Ronald S. Rock[1], W. Marshall Stark[2], Martin R. Boocock[2] and Phoebe A. Rice[1,*]

[1]Department of Biochemistry and Molecular Biology, the University of Chicago, Chicago, IL 60637, USA and [2]Institute of Molecular Cell and Systems Biology, University of Glasgow, Glasgow G128QQ, UK

Received September 20, 2017; Revised December 18, 2017; Editorial Decision December 19, 2017; Accepted December 20, 2017

ABSTRACT

Members of the serine family of site-specific recombinases exchange DNA strands via 180° rotation about a central protein-protein interface. Modeling of this process has been hampered by the lack of structures in more than one rotational state for any individual serine recombinase. Here we report crystal structures of the catalytic domains of four constitutively active mutants of the serine recombinase Sin, providing snapshots of rotational states not previously visualized for Sin, including two seen in the same crystal. Normal mode analysis predicted that each tetramer's lowest frequency mode (i.e. most accessible large-scale motion) mimics rotation: two protomers rotate as a pair with respect to the other two. Our analyses also suggest that rotation is not a rigid body movement around a single symmetry axis but instead uses multiple pivot points and entails internal motions within each subunit.

INTRODUCTION

Serine recombinases are a family of site-specific DNA recombinases that rearrange DNA by an unusual mechanism involving rotation about a relatively flat, hydrophobic interface within a multimeric catalytic module (Figure 1; reviewed in (1)). This mechanism is unprecedented: although other macromolecular systems such as the bacterial flagellum and the F_1F_0 ATPase also have components that can rotate a full 360° relative to other components, they involve rotation of a stalk within a sheath rather than a molecular swivel in which half of the entire complex rotates relative to the other half.

Our model system is Sin, a member of the 'small' serine recombinase sub-family (2). Sin is encoded on ∼50% of staphylococcal plasmids, many of which also encode antibiotic resistance (3,4). Sin is presumed to resolve plasmid dimers (that result from replication restart) into monomers, as has been demonstrated for related enzymes (5,6). Other well-studied small serine recombinases include the resolvases encoded by the γδ and Tn3 transposons and the DNA invertases Gin and Hin (reviewed in (1,7,8)). The other major group of serine recombinases, termed 'large' for their larger DNA binding domains, serve as integrases for some bacteriophages and mobile genetic elements (9). Members of both subfamilies are used as biotechnology tools. They catalyze rearrangements such as insertions, deletions and inversions at specific DNA sequences without relying on the hosts' DNA repair machinery, and for resolvases such as Sin, chimeric proteins with 'designer' specificity can be engineered (10,11).

In the prevailing model for strand exchange, two serine recombinase dimers bind two double-stranded DNAs at conserved crossover sites (reviewed in (1)). Upon tetramerization, the recombinase makes double-stranded breaks in both DNA duplexes. The cleavage reaction employs a nucleophilic serine to displace a DNA 3'O, forming an intermediate in which each protein subunit is covalently linked to a broken DNA end. To exchange strands, one half of the protein-DNA complex swivels 180° relative to the other half (Figure 1). The religation reaction is the reverse of the cleavage reaction. No high energy cofactors (such as ATP) or divalent cations are required.

Serine recombinases are generally regulated by controlling the step at which two crossover site – bound dimers are converted to a catalytically active tetramer. This step requires large conformational changes, which lead to weaker interactions of each individual subunit with its initial dimerization partner, and tighter interactions with a new partner to form the 'rotating dimers' that move together during recombination (the green–yellow, and blue–purple pairs in Figure 1). For resolvases such as Sin, this is triggered by assembly of a larger complex termed a 'synaptosome'. The synaptosome includes the crossover-site bound subunits plus additional proteins and DNA; for Sin, two additional Sin dimers and two copies of the DNA bending protein HU are needed, whereas other serine resolvases such as γδ and Tn3 use four additional resolvase dimers (see (12) for a structure-based model of the Sin synaptosome). The synaptosome serves as a topological filter to ensure that recombination occurs exclusively between the appropriate partner sites, aligned in the appropriate orientation to achieve plasmid dimer resolution (rather than inversion

*To whom correspondence should be addressed. Email: price@uchicago.edu

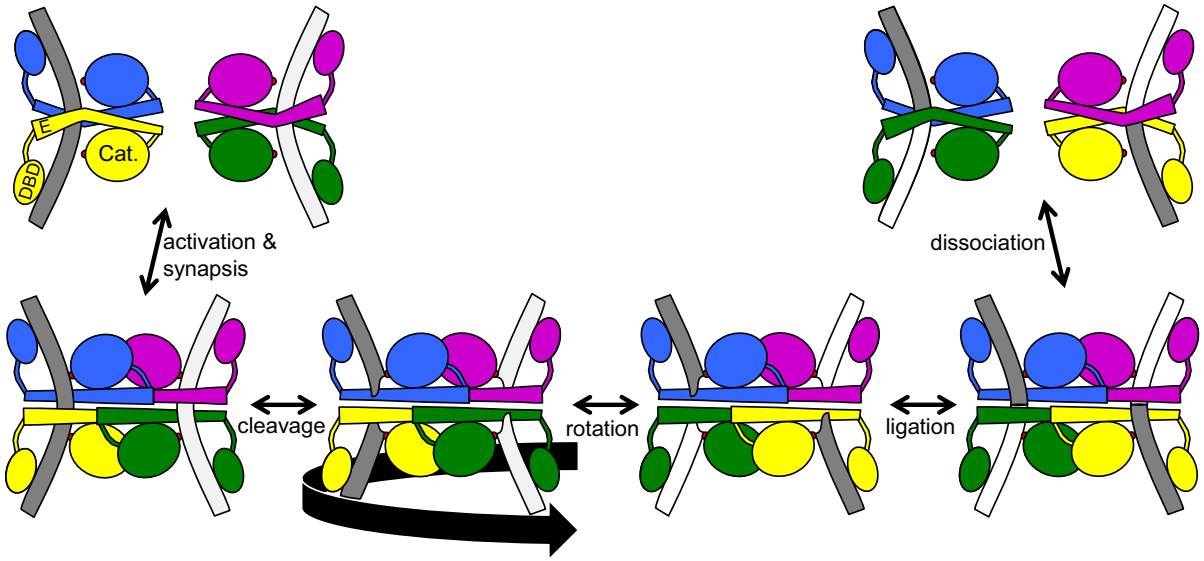

Figure 1. Recombination by serine recombinases. The cartoon shows the catalytic domain core ('cat') and the DNA binding domain ('DBD') of each subunit linked by helix E. Two protein dimers each bind a double-stranded crossover site DNA, then interact to form a tetramer. Tetramerization is usually triggered by other factors, but is rendered spontaneous by the activating mutations used in this study. It entails a large conformational change in which the E helices repack relative to the catalytic core. A double-strand break is then made in each crossover site, after which half of the complex (one 'rotating dimer,' here the lower two subunits shown in yellow and green) rotates relative to the other half to exchange DNA strands. DNA strands can be religated after every 180° of rotation. Small red spheres mark the active site serines.

of the intervening segment, or insertion of one plasmid into another) (12,13). In the context of the synaptosome, unidirectional (right-handed) rotation is driven by relaxing supercoils (14). Other small serine recombinases are regulated by similar sets of accessory factors. However, many constitutively active mutants of Sin and other serine recombinases have been identified (15–20). These mutants escape regulation and recombine crossover site-carrying DNAs in the absence of accessory factors. Some of these have been shown to form tetramers *in vitro* even in the absence of DNA (21). These mutants can also recombine linear DNAs *in vitro,* proving that thermal energy is sufficient to drive rotation, although thermal energy alone cannot favor one direction of rotation over the other.

A wealth of data supports the rotational mechanism for strand exchange (1). For example, rotation explains the carefully-measured changes in plasmid topology introduced by recombination (14). Multiple rounds of recombination (without dissociation of the synaptosome) result in defined product topologies after rotation of 180°, 360°, 540°, 720°, etc, and when the two base pairs at the centers of the crossover sites differ such that religation after 180° would create mismatches, the 360°-rotated product is formed with no intermediate DNA religation or rearrangements of the proteins as would be required for any mechanism that does not involve rotation (13,22–25). Rotation has also been observed in real time in single molecule experiments (26–28). The velocity measured in such experiments depends upon torque but when examined under similar conditions, DNA relaxation induced by a serine recombinase was slower than that induced by a type IB topoisomerase (29).

Serine recombinases have a modular architecture: one domain, usually C-terminal, is required for sequence-specific DNA binding, and the other, termed the catalytic domain, is responsible for catalysis, oligomerization, and rotation but does not bind DNA strongly in isolation. The core of the catalytic domain contains a four-stranded β-sheet flanked by four α-helices (30). A fifth helix, termed helix E, is connected to the core by a highly flexible linker and is not required for folding of the core (31). The catalytic domains formed dimers in crystal structures of WT small serine recombinases (with and without the DNA binding domains), whereas they formed tetramers in structures of constitutively active mutants (12,32–37). In both oligomeric states, helix E is at the center of the interface with other subunits. However, the conformational change between the dimeric and tetrameric states extensively remodels helix E's inter- and intramolecular interactions.

All the tetramer structures have a central flat, hydrophobic interface formed primarily by interactions between two pairs of antiparallel E helices. The largest difference among these structures is that one half of the tetramer is rotated about this interface with respect to the other half. The first structure of an activated serine recombinase mutant was of full length γδ resolvase, which crystallized with crossover site DNA in a post-cleavage conformation (33). In this and other independent structures of activated γδ resolvase tetramers (including a Hin-γδ chimaera with DNA and an isolated catalytic domain), and in a structure of the catalytic domain of TP901–1 integrase, whether or not DNA and the DNA-binding domain were present, the two pairs of antiparallel E helices cross at approximately 85° (34,38). However, subsequent structures, using activated variants of different serine recombinases, showed different crossing angles: 50° for the Sin R54E/Q115R catalytic domain and ∼127° for an activated Gin catalytic domain (35,36). Additionally, crosslinking of Hin residues during recombination

detected a state in which the crossing angle is ∼0° (39). Although all the active tetramers have approximate 222 symmetry (i.e. three mutually perpendicular twofold axes that intersect in one central point), that symmetry is perfect only in the lower-resolution structures. The Sin R54E/Q115R structure probably represents the closest approximation to the 0°/180°-rotated cleavage- and religation-ready state because uncleaved DNA could be docked onto it, with both scissile phosphates aligned with the active sites, whereas in other tetrameric structures the active sites are too far apart to do so (36,37).

Taken together, the biochemical and structural evidence strongly support recombination via rotation, but very little data existed to describe the mechanics of the rotational movement itself. Additional questions remained: if each serine recombinase can presumably adopt any rotational conformation, why has each recombinase been observed in only one rotational state? Do the rotating halves of the tetramer move as rigid bodies, or do the individual subunits flex during rotation? Is rotation through 180° smooth, or does it proceed through transient, metastable states? Does the active site remain fully assembled throughout rotation?

In this study, we address these questions using a combination of x-ray crystallography and normal mode analysis. We report four new crystal structures of the catalytic domains of constitutively active mutants of Sin that highlight the fluid nature of the tetramer interface. The most striking of the new structures is that of Sin R54E/I113V, which shows two distinct rotational states for the same recombinase, within the same crystal. Additionally, normal mode analysis (42) predicts that the most likely large-scale conformational change that these structures would undergo in solution corresponds to the expected rotation. Our findings provide new, strong support for the rotational model of strand exchange, and also provide new insight into how it occurs: inter-dimer contacts can be optimized throughout rotation by flexibility in the outer regions of the interface and by using a series of slightly different pivot points.

MATERIALS AND METHODS

Selenomethionine protein expression and purification

Activating mutations were cloned into the plasmid pSA1162, which encodes the N-terminal domain (residues 1–128, with no additional tags) of pI9789 Sin recombinase. The resulting plasmids were transformed into Rosetta (DE3)[pLysS] (Novagen) cells. Colonies were inoculated into a 40 ml starter culture in Luria broth with 0.04% glucose, 50 μg/ml kanamycin and 33 μg/ml chloramphenicol. The starter culture was grown at 37°C and 300 rpm until OD_{600} was 0.4–0.5, then cells were spun down at ∼750 g in a swinging bucket rotor at 4°C and resuspended in 40 ml M9 minimal medium (Fisher Scientific) with additives (0.04% glucose, 10 mM sodium chloride, 0.1 mM calcium chloride, 2 mM magnesium sulfate and 1 mg/ml thiamine). The resuspended cells were split between two 1-L flasks of M9 media with additives. When the 1-L cultures reached an OD_{600} of 0.4–0.5, a six amino acid cocktail was added to a final concentration of 100 mg/l of each of L-isoleucine, L-leucine, L-lysine, L-phenylalanine, L-threonine and L-valine, and selenomethionine was added to a final concentration of 60 mg/l. The culture was grown for another 15 minutes, then expression was induced with 0.5 mM isopropyl β-D-1-thiogalactopyranoside for 3 h. The cells were harvested via centrifugation, then stored at –20°C. Cell pellets were resuspended in 50 ml lysis buffer (25 mM Tris pH 8.0, 10 mM NaCl, 1 mM EDTA, 1 mM dithiothreitol (DTT) and Roche complete mini protease inhibitor), then sonicated to lyse the cells. Cells were centrifuged at 18 000 rpm in an SS-34 rotor for 30 min. The pellet was resuspended in wash buffer (25 mM Tris pH 8.0, 1M NaCl, 1 mM EDTA, 1 mM DTT and one tablet per liter Roche complete mini protease inhibitor) and spun down again at 18 000 rpm for 30 min in the SS-34 rotor; this wash step was repeated twice. The final pellet was resuspended in buffer A (25 mM Tris pH 8.0, 10 mM NaCl, 1 mM EDTA, 3 M urea and 1 mM DTT) then centrifuged at 18 000 rpm for 30 min. The soluble fraction contained denatured Sin, which was filtered with a 0.22 μm vacuum filter, then loaded onto a Q FF anion exchange column (Amersham). Protein was eluted using a gradient of buffer B (25 mM Tris pH 8.0, 2 M NaCl, 1 mM EDTA, 3 M urea and 1 mM DTT). The fractions containing Sin were pooled and dialyzed into buffer C (25 mM Tris pH 8.0, 2 M NaCl, 1 mM EDTA, 2 M urea and 1 mM DTT). Sin was refolded via several successive dialysis steps into the following buffers: (i) buffer D (buffer C with 1 M urea), (ii) buffer E (buffer C with no urea), (iii) buffer F (25 mM Tris pH 8.0, 1 M ammonium sulfate, 1 mM EDTA, and 1 mM DTT), then two dialysis steps in storage buffer (25 mM Tris pH 8.0, 0.5 M ammonium sulfate, 1 mM EDTA, 1 mM DTT and 5% glycerol). Each liter of culture yielded 50–60 mg of protein. Each mutant was concentrated to ∼100 mg/ml using Amicon centrifugal filters (10 000 MWCO cutoff), aliquoted, and stored at –80°C.

Crystallization

Sin R54E/I113V catalytic domain crystals were grown using the hanging drop vapor diffusion method. Protein stocks were diluted 1:10 in 25 mM HEPES pH 7.0 and 500 mM $(NH_4)_2SO_4$, then mixed 1:1 with well solution. Sin R54E/I113V grew in large, disordered spheres after a month in 0.1 M HEPES pH 7.0, 1.38–1.5 M $(NH_4)_2SO_4$, 8% PEG 400 and 10 mM DTT at 19°C. These crystals were streak-seeded using horse hair into new drops containing a 1:1 mix of diluted protein and well solution (100 mM HEPES pH 7.0, 1.41 M $(NH_4)_2SO_4$, 6% PEG 200 and 10 mM DTT) at 19°C, but after several months, trays were kept at room temperature due to incubator failure. Streak seeded crystals were more regular but very small after eight months, so the 2 μl drops were aspirated and diluted into 500 mM $(NH_4)_2SO_4$. New trays were set up with drops containing 0.5 μl diluted microcrystals, 1.1 μl protein stock (diluted 1:10 as in previous trays), and 1.1 μl well solution (200 mM HEPES pH 7.0, 1.35 M $(NH_4)_2SO_4$, 5% PEG 200, 1 mM DTT and 5% propylene glycol) at room temperature. Crystals grew to ∼0.1 μm. Crystals were frozen in liquid nitrogen without additional cryoprotection. Diffraction data were collected from a single crystal at the GM/CA beamline 23-ID-B at Advanced Photon Source (APS) at Argonne National Laboratory in Lemont, IL.

Crystallization of the Sin R54E/I100T, Sin R54E/I100T/Q115R and Sin R54E/T77I/I100T/Q115R catalytic domains was more straightforward. Each of these crystals grew in less than a week using the hanging drop vapor diffusion method. All catalytic domain stocks were diluted 1:10 and mixed 1:1 with a reservoir solution and incubated at 19°C. Sin R54E/I100T grew in a well containing 10 mM DTT, 50 mM HEPES pH 7.0, 1.77 M $(NH_4)_2SO_4$, 13% PEG400 and 5% propylene glycol; the crystal was dipped into a similar solution containing 10% propylene glycol prior to freezing with liquid nitrogen. Sin R54E/I100T/Q115R was grown over a well containing 10 mM DTT, 50 mM HEPES pH 7.0, 1.92 M $(NH_4)_2SO_4$, 8% PEG 400 and 10% propylene glycol; the crystals were frozen without additional cryoprotection. Sin R54E/T77I/I100T/Q115R was grown over a well containing 10 mM DTT, 500 mM HEPES pH 7.0, 0.96 M $(NH_4)_2SO_4$, 8% PEG 400; the crystals were dipped into the same buffer supplemented with 10% propylene glycol for cryoprotection prior to freezing. Diffraction data for all three mutants were collected at the SBC 19-ID-D beamline at APS.

All data sets were indexed and scaled using the HKL2000/3000 suites (40). As the data were originally processed to higher resolution than was used in refinement, data were later rescaled using the 'no merge original index' option to obtain appropriate merging statistics in the outermost bins for Table 1. Anisotropic resolution limits were estimated using the anisotropy server (41). The Sin R54E/I100T, R54E/I100T/Q115R, and R54E/T77I/I100T/Q115 structures were solved using Phaser molecular replacement in the Phenix suite, using a monomer from the Sin R54E/Q115R structure as the search model (PDBid 3pkz) (36,42). The Sin R54E/I100T B-factors are significantly higher than is typical for structures of this resolution. Therefore, although the main chain density is well-defined in most parts, the electron density for many side chains is poor. The Sin R54E/I113V structure was phased by molecular replacement using Phaser and using a rotating dimer from our R54E/I100T structure as the search model. The slightly different rotating dimer conformation observed in the absence of the Q115R change explains why the I113V structure could be solved by using a rotating dimer from the I100T structure but not the Q115R structure for molecular replacement. Successive rounds of refinement were primarily carried out in Phenix. However, we utilized the Sosnick lab's Godzilla torsion angle optimization and real-space refinement server to optimize our model's geometry at several points during refinement (43). Twofold NCS restraints were used in refining the I100T/Q115R structure. All models were built with Coot (44).

Rotation angles were calculated using only the E helices as guides because that is where the electron density is most well-defined and because the relative orientation of the E helix to the catalytic core is somewhat variable.

To calculate buried surface areas, we substituted methionine for selenomethionine in the structures and calculated accessible hydrophobic surface areas using NACCESS (45). For each tetramer, we calculated solvent-accessible hydrophobic surface area of each rotating dimer separately, then subtracted that of the intact tetramer.

Normal mode analysis

Normal mode analysis was performed using the ElNemo server (46). The default cutoff for elastic residues was 8 Å. Minimum and maximum perturbations were selected to show the greatest range of motion without disrupting the secondary structure. NRBL, the number of residues grouped together in calculations, was set to 1.

All structure figures were made using PyMOL (The PyMOL Molecular Graphics System, Version 1.8 Schrödinger, LLC).

RESULTS

Structure determination

The catalytic domains (residues 1–128) of four constitutively active Sin mutants (I113V, I100T, 100T/Q115R, and T77I/I100T/Q115R) were expressed in *Escherichia coli* grown with selenomethionine, purified, and crystallized as described in the methods section. As for our previous Sin Q115R structure, all variants also included the R54E mutation, which improves solubility but does not significantly affect catalytic activity (for simplicity, this substitution is omitted in further descriptions) (20). Mutations were selected from a large collection of constitutively activating substitutions that map to different inter- and intramolecular contacts in Sin structures (12,20,36). I113V was chosen because of its strong activating effect and intriguing location within the flat interface (20). T77I/I100T/Q115R was chosen because when mixed with crossover site DNAs *in vitro*, it stabilized synaptic complexes that migrated differently in gels from those formed with the Q115R single mutation, suggesting a different rotational state or different dynamics within the tetramer (20). We also previously characterized the biochemical properties of the I100T and Q115R variants (21). For the strongly activated Q115R protein, we found by analytical ultracentrifugation that it is ∼50% tetrameric (with and without DNA) at 800–900 nM [Sin], that the recombination rate is highly concentration-dependent, and that the steepest part of a rate versus concentration curve correlates fairly well with the dimer-tetramer equilibrium constant. I100T Sin is less strongly activated, largely dimeric with a tiny tetramer peak in the ultracentrifuge, and required much higher concentrations for activity.

All four structures were phased by molecular replacement, and the solutions were checked by confirming the alignment of the SeMet residues with peaks in the anomalous difference Fouriers. Refinement statistics for these structures are shown in Table 1.

Structure of Sin I113V reveals two rotational states

Crystals of Sin I113V diffracted slightly anisotropically to ∼3.2–3.3 Å and were solved by molecular replacement with a Sin I100T dimer (discussed below) as the search model. The asymmetric unit contains 12 protomers arranged into

Table 1. Data collection and refinement statistics

mutations	R54E I113V	R54E I100T	R54E I100T Q115R	R54E T77I I100T Q115R
Contents of asymmetric unit	Three tetramers	One tetramer	Half tetramer	Half tetramer
PDB ID	5c31	5c32	5c34	5c35
SBgrid data set #	146	144	143	145
Wavelength	0.9795	0.9791	0.9792	0.9791
Resolution range used in refinement	49.31–3.1 (3.21–3.1)	36.35–3.05 (3.16–3.05)	36.26–2.66 (2.75–2.66)	36.17–2.4 (2.47–2.4)
Resolution where F/sigma $F > 3$ along a,b,c[@]	3.2, 3.2, 3.3	3.3, 3.4, 3.1	2.7, 2.7, 2.7	2.6, 2.6, 2.4
Space group	$P\,2_1\,2_1\,2_1$	$C\,2\,2\,2_1$	$P\,6_5\,2\,2$	$P\,6_5\,2\,2$
Unit cell	65.59 152.72 193.75	83.77 114.19 146.35	74.01 74.01 181.95	73.84 73.84 180.48
Total reflections	256 112 (24347)	189 345 (17515)	195 825 (18366)	207 523 (9196)
Unique reflections	36 180 (3520)	13 666 (1182)	9091 (871)	12 054 (1142)
Multiplicity	7.1 (6.9)	13.9 (13.2)	21.5 (21.1)	17.2 (8.0)
Completeness (%)	99.91 (99.69)	98.37 (84.68)	99.51 (99.54)	99.53 (97.59)
Mean I/sigma(I)	9.94 (1.10)	14.76 (0.66)	41.23 (3.11)	24.43 (0.80)
Wilson B-factor	82.78	120.23	76.53	72.44
R-merge	0.242 (1.93)	0.225 (5.21)	0.083 (1.32)	0.110 (2.17)
R-meas	0.261 (2.09)	0.234 (5.42)	0.085 (1.35)	0.113 (2.31)
R-pim	0.097 (0.782)	0.063 (1.48)	0.018 (0.291)	0.027 (0.741)
CC1/2	0.994 (0.381)	0.998 (0.142)	0.999 (0.839)	0.999 (0.202)
CC*	0.999 (0.743)	1 (0.498)	1 (0.955)	1 (0.58)
Reflections used in refinement	36179 (3520)	13460 (1122)	9090 (872)	12030 (1136)
Reflections used for R-free	1890 (184)	1349 (115)	472 (28)	1204 (112)
R-work	0.228 (0.347)	0.265 (0.423)	0.294 (0.407)	0.316 (0.485)
R-free	0.287 (0.371)	0.312 (0.448)	0.308 (0.448)	0.336 (0.450)
CC(work)	0.947 (0.587)	0.959 (0.297)	0.917 (0.622)	0.940 (0.373)
CC(free)	0.943 (0.460)	0.934 (0.112)	0.899 (0.502)	0.916 (0.607)
Number of non-hydrogen atoms	12 305	4015	1953	2005
Macromolecules	12 160	3995	1936	1993
Ligands	105	20	15	10
Solvent	40		2	2
Protein residues	1501	492	239	248
RMS(bonds)	0.001	0.003	0.004	0.003
RMS(angles)	0.46	0.56	0.77	0.55
Ramachandran favored (%)	97.02	95.21	94.42	94.58
Ramachandran allowed (%)	2.85	4.58	5.58	5.42
Ramachandran outliers (%)	0.14	0.21	0.00	0.00
Rotamer outliers (%)	0.51	0.00	0.45	0.00
Clashscore	24.12	1.23	3.54	1.97
Average B-factor	92.88	142.31	115.19	133.05
Macromolecules	92.61	142.43	115.20	133.05
Ligands	134.55	118.88	116.26	141.59
Solvent	64.62		99.55	91.48
Number of TLS groups	78	8		12

Statistics for the highest-resolution shell used in refinement are shown in parentheses.
[@] determined by the Anisotropy server (41).

three tetramers. Within these tetramers, the backbone structures of the six 'rotating dimers' (the pairs of subunits expected to move together during rotation) are all quite similar except for variations in the flexible loop (residues 95–103) between the core and helix E, and small adjustments in the position of helix E. However, the relative orientations of the rotating dimer pairs comprising each tetramer vary (Figure 2).

Two of the three I113V tetramers (subunits ABCD and EFGH) adopted a rotational state similar to that previously observed for Sin Q115R (the presumably unrotated state), with the two pairs of antiparallel E helices crossed at 45–48° (36). However, in the third tetramer (subunits IJKL) the crossing angle is only 15°. This is the first time that two rotational states have been observed for any individual serine recombinase, and comparison of these two states is particularly well-controlled because they are the same constitutively active mutant and in the same crystal.

Within the limits of our resolution, the active site appears to be fully assembled in all three Sin I113V tetramers—that is, all the catalytic arginine residues coordinate a sulfate ion that binds where the scissile phosphate was seen in activated γδ resolvase—DNA structures. Previously, similarly assembled active sites were seen only in the 'unrotated' Sin Q115R structure. In addition to the nucleophilic serine (Ser9 for Sin), serine recombinase active sites include an arginine-rich binding pocket for the scissile phosphate; this is occupied by a sulfate ion in our structures. In inactive dimers Arg 69, which is the likely general acid for the cleavage reaction, is flipped away from the active site pocket, whereas in the I113V and Q115R Sin tetramers, it has moved to interact with the sulfate ion (12,36,47).

Further variation revealed by three additional structures

Crystals of Sin I100T contained a single tetramer in the asymmetric unit and diffracted anisotropically to 3.4–3.1 Å. Phases were determined by molecular replacement using a single subunit of Sin Q115R as a model. Two additional crystal forms of Sin I100T were solved but not pursued further because the overall structure was similar but the resolution was lower. The rotational state of this tetramer (crossing angle 59–60°) differs by ∼10–15° from that of Sin Q115R and Sin I113V tetramers ABCD and EFGH (Figure 3A and B). This represents a third observed rotational state for Sin.

The Sin I100T/Q115R and T77I/I100T/Q115R structures are nearly identical (Figure 3C and D). They crystallized in the same space group, with two subunits in the

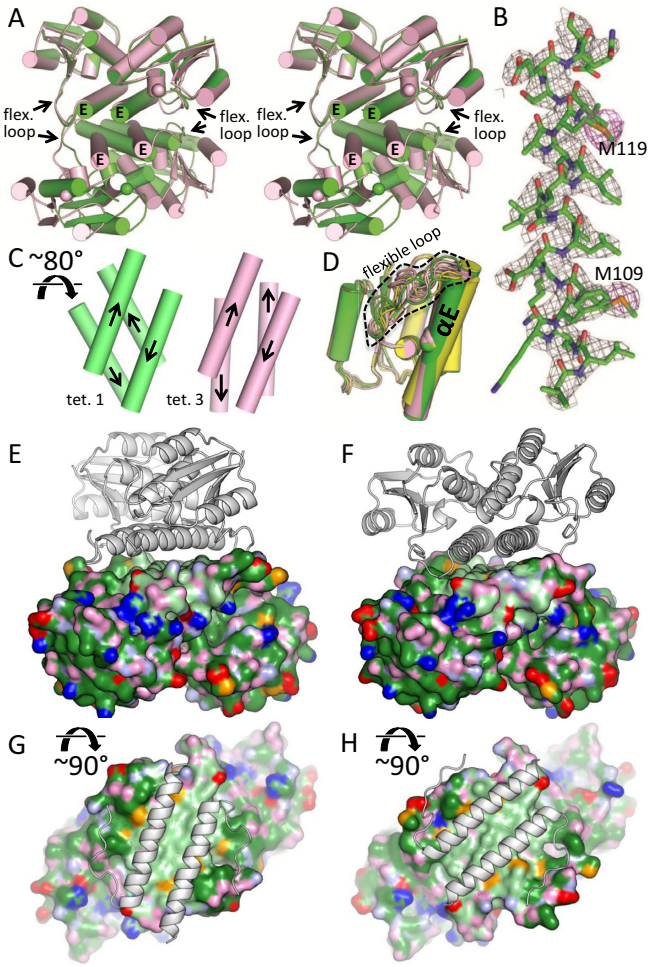

Figure 2. I113V crystals contain tetramers in two different rotational states. (**A**) Stereo pair showing I113V tetramers 1 (subunits ABCD, green) and 3 (subunits IJKL, pink), superimposed using the E helices of the upper rotating dimer as guides. The hydroxyl groups of the catalytic serines are marked with spheres. Tetramer 2 (subunits EFGH; not shown) is nearly identical to tetramer 1. (**B**) The central portion of Helix E of subunit A is shown. The final weighted 2Fo-Fc (gray) and anomalous difference (magenta) electron density maps are shown contoured at 1.5σ and 3.5σ and using carve radii of 1.7 and 2, respectively. (**C**) Only the E helices from the two tetramers in part a are shown, viewed from above relative to part a, with the plane of the rotational interface now parallel to the plane of the page. Arrows indicate the directionality of the helices. (**D**) Eleven I113V subunits aligned by their cores, showing the flexibility between the E helix and the core. ABCD are green, EFH yellow, IJKL pink. Subunit G was omitted because the model is missing the flexible loop. Sphere highlights the position of V113. (E, F). Tetramers 1 (**E**) and 3 (**F**) are shown with the lower rotating dimer in surface representation, colored according to atom type: C atoms within helix E pale green and other C green, Se orange (in SeMet residues), charged O red and uncharged O pink, charged N blue and uncharged N light blue. The overall orientation is similar to that in part (A), but in this case the two tetramers were superimposed using the lower two rotating dimers as guides before preparing the individual figures. (**G**, **H**) The representations in parts (E) and (F) from an orthogonal viewpoint and with only the E helices of the upper rotating dimer shown.

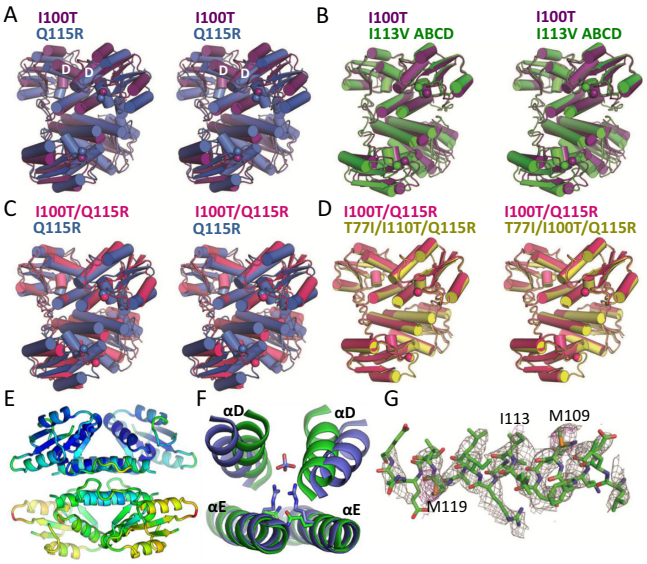

Figure 3. Further variability seen in additional Sin tetramer structures. (**A**–**D**). Stereo views of pairwise comparisons, in which tetramers were superimposed using the E helices of the upper rotating dimers as guides, and spheres mark the catalytic serines. (A) I100T (purple) vs. Q115R (blue) (36). (B) I113V tetramer 1 (green) vs. I100T (purple). (C) I100T/Q115R (pink) versus Q115R (blue) (D) I100T/Q115R (pink) versus T77I/I100T/Q115R (yellow). (**E**) The T77I/I100T/Q115R structure is shown colored according to relative B factors, shaded from blue (lowest) to red (highest). (**F**) Close-up of only the D and E helices from one rotating dimer of Sin Q115R (blue) and I113V (green), showing how the nature of the side chain at position 115 (sticks) alters the spacing of the D helices. Also shown is a sulfate ion that interacts with R115 in the Q115R-including structures. (**G**) Experimental electron density for the E helix of Sin T77I/I100T/Q115R (subunit A), calculated from Se SAD phases and contoured at 1.5σ, is shown in gray. Anomalous difference density contoured at 4.0σ is also shown in magenta.

asymmetric unit, and diffracted isotropically to 2.7 Å and anisotropically to 2.6–2.4 Å, respectively. These structures were solved by molecular replacement using a Sin Q115R monomer as a search model. As additional verification, we later calculated experimental phases using the known positions of the Se atoms (Figure 3G). Crystallographic symmetry reconstructs a tetramer in which the E helices cross at 60°. Each polypeptide chain forms a rotating dimer with its own symmetry mate: that is, with respect to Figure 1, the asymmetric unit corresponds to one blue plus one green subunit, and a crystallographic twofold axis runs vertically through the center of the complex. In both structures, one rotating dimer has a lower average B-factor than the other: 114 versus 180 for T77I/I100T/Q115R and 112 versus 144 for I100T/Q115R. Furthermore, the B-factors for the less well-ordered dimer are lowest at the center of the flat interface, and highest at the periphery (Figure 3E). This suggests that one dimer is relatively firmly locked in place by crystal packing whereas its partner samples an ensemble of similar but non-identical rotational orientations. This epitomizes the difficulties in crystallizing active serine recombinases, but has mechanistic implications: it suggests that even within a particular rotational sub-state, the local energy well may be rather broad and shallow.

Comparison of activated Sin structures

Among the multiple determinations of the monomer structure, the most variable region is the loop that connects the core to helix E (Figure 2D). This loop forms the periphery of the tetramer interface, and our normal mode analysis

(described below) suggests that flexibility in this loop may help avoid steric clashes with DNA overhangs and other protein loops during rotation. The hydrophobic side chains that protrude from helix E into the rotational interface also adopt different rotamers on different subunits and in different rotational states, most notably the large but highly flexible M109 and M119.

The structures of rotating dimers can be grouped into two categories based on the distance between their D helices, which correlates with the presence or absence of the Q115R mutation (Figure 3A–D). When Q115R is not present (Sin I100T, Sin I113V) the D helices within a rotating dimer pack against one another, similar to the architecture of γδ and Gin rotating dimers, with the amides of the two copies of Q115 hydrogen bonded to one another (Figure 3f) (34,35). When Q115R is present, subtle shifts in the inter- and intra-molecular interactions of helix E move the two D helices ∼4 Å apart to accommodate the tips of the Arg115 side chains and the sulfate ion that interacts with them. As Q115R is the most activating single mutation isolated for Sin, this conformational shift is unlikely to be deleterious to catalytic activity (20).

None of the five Sin tetramer structures now available exhibit perfect 222 symmetry (which entails three mutually perpendicular twofold axes that intersect at a single point). For instance, in all three I113V tetramers, the internal twofold axes of the two rotating dimers are offset from one another by several angstroms rather than being co-linear (Figure 4). For the I110T/Q115R and T77I/I100T/Q115R tetramers, in which the internal twofold axes of the rotating dimers coincide with a crystallographic twofold axis, that axis and the other local symmetry axes do not intersect at a common point and sometimes involve a translational ('screw') component. Furthermore, even tetramers that have a similar overall rotational conformation vary in detail (e.g. Q115R versus I113V tetramer 1). When the E helices from one rotating dimer of each structure are aligned, the other pair of E helices sample an array of angles (Figure 4E). This variability (along with the *B*-factor variability noted above) suggests that the states seen in our crystals reflect broad, shallow minima in the rotational energy landscape.

How do the activating mutations used here exert their effects? The mutated residues make different interactions in the active tetramer structures than they do in the inactive WT dimer structure (Supplementary Figure S1), which supports the idea that their mutation tips the energetic balance between the two conformations. Quantifying their expected effects on the stability of each conformation is difficult for several reasons: the mutations used here are quite subtle (Ile versus Val or Thr), the electron density is sometimes unclear for the tips of the side chains in question, and due to imperfect symmetry in the dimer as well as the tetramer structures, the details of the interactions these residues make are slightly different in each subunit. However, the sum of these small changes in each subunit must be sufficient to favor tetramer formation even in the absence of the accessory factors that WT Sin requires.

Surface area burial of different states is similar

To address whether or not one rotational state is significantly more favorable than the others, we calculated the hydrophobic surface area that is buried in the Sin I113V rotational interfaces, which can be taken as a rough proxy for energy (48,49). We focused on the different Sin I113V tetramers to avoid confounding effects due to different activating mutations. For each tetramer, we calculated the sum of the hydrophobic surface area of two rotating dimers minus that of the tetramer. The rotational interfaces of the Sin I113V ABCD and IJKL tetramers differ by only 5%: they bury 2499 and 2374 $Å^2$ of hydrophobic surface area, respectively. For comparison, in the Q115R structure, tetramers ABCD and IJKL (which are nearly identical to one another) bury 2636 and 2621 $Å^2$. These data support the hypothesis that the two I113V tetramers represent energetically similar minima in the rotational landscape.

Normal mode analysis

To examine the most energetically accessible large-scale motions that Sin tetramers are likely to undergo, we used the ElNémo server to predict their normal modes (46). This server approximates the protein's potential energy function around an initial state using an elastic network model essentially consisting of simple springs that mimic the connections between amino acids. A simple Hookean potential is applied to all atoms in the structure, and the matrix of mass-weighted second derivatives is diagonalized to give eigenvectors (modes) and eigenvalues (frequencies). Although the explicit values for the speed and amplitude of motion are arbitrary in such calculations, the lowest frequency modes are likely to describe the direction of biologically relevant conformational changes. In a survey of 3814 proteins with an open and closed state in the PDB, approximately half of the transitions were described by one or both of the first two normal modes (48). In other studies, a superposition of the lowest-frequency normal modes described the changes between the open and closed state of a protein and predicted conformational changes in DNA polymerases and other systems (49,50).

The first non-trivial normal modes for both Sin I113V tetramer conformations describe rotation: the two rotating dimers swivel with respect to each other at the rotational interface (Figure 5 and supplementary movie 1). The two antiparallel E helices of each rotating dimer remain paired. However, in addition to the overall rotation seen within the tetramer, the core of each subunit moves with respect to its E-helix (Figure 5C). This intramolecular motion agrees with the flexibility seen in our crystal structures and with the dramatic shifts between the core and helix E that occur in the dimer to tetramer transition (compare Figures 2D and 5C and Supplementary Figure S1) (51). Flexibility in the helix E-core connector loop may allow the Sin structure to 'breathe' in order to transition between low energy states in the rotation pathway. The ElNemo server returns very similar results for normal mode analysis of the other structures reported here, and of the tetrameric catalytic domains of two other serine recombinases: activated Gin invertase (PDBID 3UJU) and γδ resolvase (PDBID 1ZR2) (Supplementary Figures S2 and S3). The DNA and DNA bind-

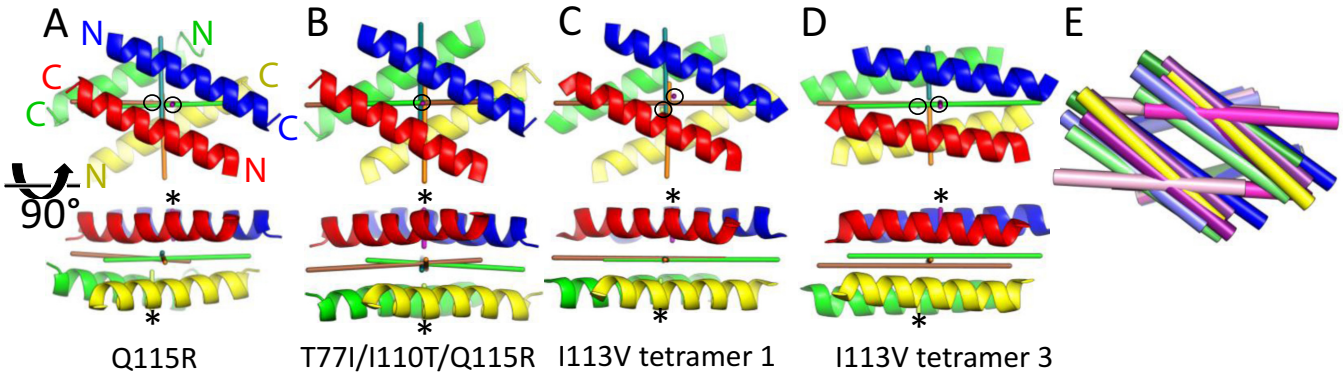

Figure 4. Variable deviations from 222 symmetry show a slippery rotational interface. (**A**–**D**). The E helices (aa 103–124) of four different tetramers are shown, oriented such that the rotational interface is parallel to the plane of the page (top) or perpendicular (bottom). Approximate twofold axes between individual pairs of E helices were obtained by sketching a line through the midpoints between pairs of Cα atoms. Axes are colored according to the pairs of E helices related by them: blue-green between the blue and green helices, brown between the red and green helices, etc. Note that some pairs of helices (e.g. blue and yellow in parts A, C and D) are related by a small translation as well as a ∼180° rotation. Circles (upper panels) and asterisks (lower panels) highlight the positions of the short purple and lime vertical axes relating the two helices of each rotating dimer. (**E**) The E helices of the different Sin tetramer structures, each aligned using the E helices of the bottom rotating dimer as guides in two ways (e.g. subunits AB of one structure aligned to subunits AB of the other, and subunits CD of one aligned to subunits AB of the other). Colors correspond to those in Figures 2 and 3e: Q115R is blue; I113V green and pink; I100T purple; T77I/I100T/Q115R yellow (I100T/Q115R is not shown as it is similar to T77I/I100T/Q115R).

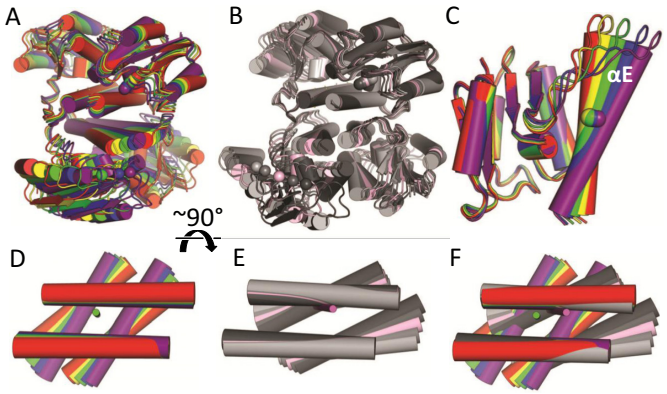

Figure 5. Normal mode analysis of Sin I113V tetramers. (**A**, **B**) Snapshots showing that the first non-trivial normal modes predicted for tetramer 1 (rainbow colors) and 3 (grayscale) mimic rotation. The initial tetramer 1 model is shown in green; maximum displacements are shown in red and purple. The initial tetramer 3 model is shown in pink; maxima are the darkest and lightest colors. Spheres mark the catalytic serines. In both cases, the individual structural models for each snapshot were superimposed using the E helices of the upper rotating dimers as guides. (**C**) An alignment of five snapshots from the predicted trajectory shown above for subunit A of tetramer 1, showing the flexibility between the E helix and the protein core. The sphere marks V113. (**D**, **E**) The same superpositions as in (A) and (B), but with only the E helices shown, with the rotational interface parallel to the plane of the page, and with predicted pivot axes shown in green and pink, respectively. (**F**) Superposition of (D) and (E).

ing domains were removed from the γδ structure to prevent small fluctuations in those regions from dominating the normal modes. The first normal modes of both structures show rotation about the central interface, and also show the core of each monomer flexing with respect to the E helix.

The exact location of the pivot axes for the predicted local swiveling motions is variable, as shown in Figure 5 for the two I113V tetramers. Although the detailed reasons for this variability are unclear, it correlates with the other signs of plasticity noted in the rotational interface, such as the variability of the dimer–dimer orientation even when the overall crossing angles are similar, the flexibility of the loop leading into helix E, and the variability of the rotamers adopted by side chains at the interface. These observations imply that, rather than smoothly rotating 180° about a single twofold axis, Sin tetramers may stochastically switch pivot points and re-optimize packing throughout rotation.

DISCUSSION

The crystal structures and normal mode analyses presented here provide strong support for the hypothesis that serine recombinases rearrange DNA via subunit rotation and provide new insights into that process. Structures of serine recombinase tetramers are now available that map out 180° of rotation, with the largest gap between snapshots being only ∼70° (Figure 6). Our structure of the catalytic domain of the constitutively active mutant Sin I113V is the first to show two different rotational states for any given serine recombinase. Since these states are seen for the same protein variant and within the same crystal, they provide a particularly well-controlled comparison of different rotational states. Furthermore, as one of two states seen for I113V is very similar to one seen for the previously reported Q115R mutant, this work disproves the hypothesis that the different rotation states reported for different serine recombinases are simply artifacts of the particular activating mutations used.

Our data also support an enhanced model of rotation during recombination. As normal mode analysis predicts that the different tetramers pivot locally about different points, and that these pivots do not correspond exactly to local symmetry axes, we propose that rotation from 0° to 180° utilizes a series of slightly different pivot points that optimize local packing and may entail small translational movements as well. Comparison of our collection of Sin tetramer structures also suggests that rotation entails reorientation of large hydrophobic side chains at the center of the

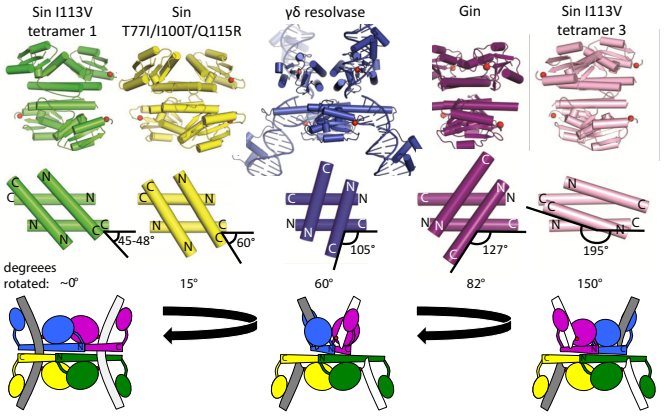

Figure 6. Snapshots of rotation provided by small serine recombinase structures. Structures of selected tetramers are shown in the top row, with active site serines denoted as red spheres. Sin I113V tetramer 1 is green, Sin T77I/I100T/Q115R yellow, activated γδ resolvase with DNA blue (33), activated Gin purple (35), and Sin I113V tetramer 3 pink. Only the E helices from each tetramer are shown in the middle panel, to highlight the different rotational states. The degrees rotated from the presumed uncut DNA-compatible state are tabulated below. The cartoons in the bottom row correspond to the different states above them.

interface, and conformational flexibility in the core–helix E connector loop at the periphery of the interface. This loop's flexibility may also allow an inchworm-like motion in which different copies of the loop within the tetramer readjust individually, so that when one copy jumps to a new position to accommodate rotation, other copies may maintain stable contacts across the rotation interface.

The existence of shallow energetic minima within the energetic landscape during rotation from 0° to 180° may be an unavoidable consequence of the knobs-into-holes model of helix-helix packing (52). Comparison of the crossing angles seen in serine recombinase tetramer structures with those tabulated in a recent survey of helix-helix crossing angles in soluble and transmembrane structures shows that the cleavage-competent Sin, rotated Sin, Gin and γδ crossing angles fall into the third, fourth, fifth and eighth most populated clusters for soluble protein structures, respectively (53). Consideration of the additional clusters may be useful for future studies modeling the full rotation of serine recombinases.

The observation that the two very different Sin I113V tetramers bury a very similar amount of hydrophobic surface implies that the already-documented minima are of roughly equal depth. Modeling of rotation based on the first γδ resolvase structure also suggested that it would not require large changes in buried hydrophobic surface area (33). Our normal mode analysis and the variability within the several structures that adopt a similar rotational state indicate that these dimples in the energetic landscape are relatively shallow. If we are correct with regards to which rotational state represents the 0°/180° point where DNA cleavage and religation occur, this implies that there is no protein-dictated 'pause point' that would favor DNA religation. This agrees with studies of other serine recombinases showing that Watson-Crick and base stacking interactions between the 2-nt 3′ overhangs at the crossover site are very important in stabilizing the complex at 0° and 180° for religation to occur (27). However, certain mutations in Hin led to accumulation of double-strand breaks, suggesting that they disrupt a protein-directed pause at 0° and 180° (54). Those observations may be reconciled if the Hin mutations in question, which change hydrophobic residues to polar or charged ones, render one rotational state more stable than the others.

Why would nature harness multiple pivot points for rotational movement, rather than simply swivel about a single axis? A one-pivot model would work best with a completely flat rotational interface, but amino acid side chains inevitably produce a surface with at least small knobs and holes. These knobs and holes may also serve a purpose: by increasing the hydrophobic surface area compared to a theoretical perfectly flat landscape, they increase the energy barrier for dissociation of the tetramer during recombination and therefore may help prevent the formation of the double-stranded breaks that dissociation would create. The asymmetry across structures and multiple pivot points may also be an unavoidable consequence of using protein to build a rotational platform. A single pivot, if it coincided with an overall twofold symmetry axis, would force the complex to pack two hills or two valleys against one another at the center. Conversely, if the same off-center pivot point were used throughout rotation, it might at some point expose part of the hydrophobic interface surface to solvent. Multiple pivot points may thus be required to allow optimal interface packing through 180° of rotation.

Finally, the variations among the multiple serine recombinase tetramer structures presented here and elsewhere suggest that rotation may not follow a single, well-defined pathway. While the rotational interface is hydrophobic and unusually flat, it is also remarkably plastic: some translational motion is clearly allowed, as is reorientation of large hydrophobic side chains and the core-helix E loop. Recombination may result from a random-walk like exploration of the many possible dimer-dimer orientations that keep the hydrophobic surface protected from solvent.

DATA AVAILABILITY

Coordinates and structure factors have been deposited with the PDB and raw crystallographic data with SBgrid. The accession numbers are: for Sin R54E/I113V, PDBid 5c31 and SBgrid data set 146; for Sin R54E/I100T, 5c32 and 144; for Sin R54E/I110T/Q115R, 5c34 and 143; for Sin R54E/T77I/I100T/Q115R, 5c35 and 145. See also Table 1.

SUPPLEMENTARY DATA

Supplementary Data are available at NAR Online.

ACKNOWLEDGEMENTS

We are extremely grateful to Sally-J. Rowland for insightful advice and comments on the manuscript. We also thank the staff of SBC and GM/CA at the Advanced Photon Source, Argonne National Laboratory, for beam time and assistance with data collection.

FUNDING

National Institutes of Health [R01 GM66011 to P.A.R., R01 GM078450 to R.S.R.]; National Institutes of Health [NIBIB 5T32EB009412 to C.S.T.] (in part). Funding for open access charge: The University of Chicago.
Conflict of interest statement. None declared.

REFERENCES

1. Stark,W.M. (2014) The serine recombinases. *Microbiol. Spectr.*, **2**, 1–16.
2. Paulsen,I.T., Gillespie,M.T., Littlejohn,T.G., Hanvivatvong,O., Rowland,S.J., Dyke,K.G. and Skurray,R.A. (1994) Characterisation of sin, a potential recombinase-encoding gene from Staphylococcus aureus. *Gene*, **141**, 109–114.
3. Shearer,J.E.S., Wireman,J., Hostetler,J., Forberger,H., Borman,J., Gill,J., Sanchez,S., Mankin,A., Lamarre,J., Lindsay,J.A. *et al.* (2011) Major families of multiresistant plasmids from geographically and epidemiologically diverse staphylococci. *G3*, **1**, 581–591.
4. Highlander,S.K., Hultén,K.G., Qin,X., Jiang,H., Yerrapragada,S., Mason,E.O., Shang,Y., Williams,T.M., Fortunov,R.M., Liu,Y. *et al.* (2007) Subtle genetic changes enhance virulence of methicillin resistant and sensitive Staphylococcus aureus. *BMC Microbiol.*, **7**, 99.
5. LeBard,R.J., Jensen,S.O., Arnaiz,I.A., Skurray,R.A. and Firth,N. (2008) A multimer resolution system contributes to segregational stability of the prototypical staphylococcal conjugative multiresistance plasmid pSK41. *FEMS Microbiol. Lett.*, **284**, 58–67.
6. Canosa,I., López,G., Rojo,F., Boocock,M.R. and Alonso,J.C. (2003) Synapsis and strand exchange in the resolution and DNA inversion reactions catalysed by the beta recombinase. *Nucleic Acids Res.*, **31**, 1038–1044.
7. Grindley,N.D.F., Whiteson,K.L. and Rice,P.A. (2006) Mechanisms of site-specific recombination. *Annu. Rev. Biochem.*, **75**, 567–605.
8. Johnson,R.C. (2015) Site-specific DNA inversion by serine recombinases. *Microbiol. Spectr.*, **3**, MDNA3–0047–2014.
9. Smith,M.C.M. (2015) Phage-encoded serine integrases and other large serine recombinases. *Microbiol. Spectr.*, **3**.
10. Olorunniji,F.J., Rosser,S.J. and Stark,W.M. (2016) Site-specific recombinases: molecular machines for the genetic revolution. *Biochem. J.*, **473**, 673–684.
11. Stark,W.M. (2017) Making serine integrases work for us. *Curr. Opin. Microbiol.*, **38**, 130–136.
12. Mouw,K.W., Rowland,S.-J., Gajjar,M.M., Boocock,M.R., Stark,W.M. and Rice,P.A. (2008) Architecture of a serine recombinase-DNA regulatory complex. *Mol. Cell*, **30**, 145–155.
13. Rowland,S.-J., Stark,W.M. and Boocock,M.R. (2002) Sin recombinase from Staphylococcus aureus: synaptic complex architecture and transposon targeting. *Mol. Microbiol.*, **44**, 607–619.
14. Stark,W.M., Sherratt,D.J. and Boocock,M.R. (1989) Site-specific recombination by Tn3 resolvase: topological changes in the forward and reverse reactions. *Cell*, **58**, 779–790.
15. Haffter,P. and Bickle,T.A. (1988) Enhancer-independent mutants of the Cin recombinase have a relaxed topological specificity. *EMBO J.*, **7**, 3991–3996.
16. Klippel,A., Cloppenborg,K. and Kahmann,R. (1988) Isolation and characterization of unusual gin mutants. *EMBO J.*, **7**, 3983–3989.
17. Burke,M.E., Arnold,P.H., He,J., Wenwieser,S.V.C.T., Rowland,S.-J., Boocock,M.R. and Stark,W.M. (2004) Activating mutations of Tn3 resolvase marking interfaces important in recombination catalysis and its regulation. *Mol. Microbiol.*, **51**, 937–948.
18. Arnold,P.H., Blake,D.G., Grindley,N.D., Boocock,M.R. and Stark,W.M. (1999) Mutants of Tn3 resolvase which do not require accessory binding sites for recombination activity. *EMBO J.*, **18**, 1407–1414.
19. Sanders,E.R. and Johnson,R.C. (2004) Stepwise dissection of the Hin-catalyzed recombination reaction from synapsis to resolution. *J. Mol. Biol.*, **340**, 753–766.
20. Rowland,S.-J., Boocock,M.R., McPherson,A.L., Mouw,K.W., Rice,P.A. and Stark,W.M. (2009) Regulatory mutations in Sin recombinase support a structure-based model of the synaptosome. *Mol. Microbiol.*, **74**, 282–298.
21. Mouw,K.W., Steiner,A.M., Ghirlando,R., Li,N.-S., Rowland,S.-J., Boocock,M.R., Stark,W.M., Piccirilli,J.A. and Rice,P.A. (2010) Sin resolvase catalytic activity and oligomerization state are tightly coupled. *J. Mol. Biol.*, **404**, 16–33.
22. Wasserman,S.A., Dungan,J.M. and Cozzarelli,N.R. (1985) Discovery of a predicted DNA knot substantiates a model for site-specific recombination. *Science*, **229**, 171–174.
23. Heichman,K.A., Moskowitz,I.P. and Johnson,R.C. (1991) Configuration of DNA strands and mechanism of strand exchange in the Hin invertasome as revealed by analysis of recombinant knots. *Genes Dev.*, **5**, 1622–1634.
24. Kanaar,R., Klippel,A., Shekhtman,E., Dungan,J.M., Kahmann,R. and Cozzarelli,N.R. (1990) Processive recombination by the phage Mu Gin system: implications for the mechanisms of DNA strand exchange, DNA site alignment, and enhancer action. *Cell*, **62**, 353–366.
25. McIlwraith,M.J., Boocock,M.R. and Stark,W.M. (1997) Tn3 resolvase catalyses multiple recombination events without intermediate rejoining of DNA ends. *J. Mol. Biol.*, **266**, 108–121.
26. Bai,H., Sun,M., Ghosh,P., Hatfull,G.F., Grindley,N.D.F. and Marko,J.F. (2011) Single-molecule analysis reveals the molecular bearing mechanism of DNA strand exchange by a serine recombinase. *Proc. Natl. Acad. Sci. U.S.A.*, **108**, 7419–7424.
27. Keenholtz,R.A., Grindley,N.D.F., Hatfull,G.F. and Marko,J.F. (2016) Crossover-site sequence and DNA torsional stress control strand interchanges by the Bxb1 site-specific serine recombinase. *Nucleic Acids Res.*, **44**, 8921–8932.
28. Xiao,B., McLean,M.M., Lei,X., Marko,J.F. and Johnson,R.C. (2016) Controlled rotation mechanism of DNA strand exchange by the Hin serine recombinase. *Sci. Rep.*, **6**, 23697.
29. Bai,H., Kath,J.E., Zörgiebel,F.M., Sun,M., Ghosh,P., Hatfull,G.F., Grindley,N.D.F. and Marko,J.F. (2012) Remote control of DNA-acting enzymes by varying the Brownian dynamics of a distant DNA end. *Proc. Natl. Acad. Sci. U.S.A.*, **109**, 16546–16551.
30. Sanderson,M.R., Freemont,P.S., Rice,P.A., Goldman,A., Hatfull,G.F., Grindley,N.D. and Steitz,T.A. (1990) The crystal structure of the catalytic domain of the site-specific recombination enzyme gamma delta resolvase at 2.7 A resolution. *Cell*, **63**, 1323–1329.
31. Pan,B., Maciejewski,M.W., Marintchev,A. and Mullen,G.P. (2001) Solution structure of the catalytic domain of gammadelta resolvase. Implications for the mechanism of catalysis. *J. Mol. Biol.*, **310**, 1089–1107.
32. Rice,P.A. and Steitz,T.A. (1994) Refinement of gamma delta resolvase reveals a strikingly flexible molecule. *Struct. Lond. Engl.*, **2**, 371–384.
33. Li,W., Kamtekar,S., Xiong,Y., Sarkis,G.J., Grindley,N.D.F. and Steitz,T.A. (2005) Structure of a synaptic gammadelta resolvase tetramer covalently linked to two cleaved DNAs. *Science*, **309**, 1210–1215.
34. Kamtekar,S., Ho,R.S., Cocco,M.J., Li,W., Wenwieser,S.V.C.T., Boocock,M.R., Grindley,N.D.F. and Steitz,T.A. (2006) Implications of structures of synaptic tetramers of gamma delta resolvase for the mechanism of recombination. *Proc. Natl. Acad. Sci. U.S.A.*, **103**, 10642–10647.
35. Ritacco,C.J., Kamtekar,S., Wang,J. and Steitz,T.A. (2013) Crystal structure of an intermediate of rotating dimers within the synaptic tetramer of the G-segment invertase. *Nucleic Acids Res.*, **41**, 2673–2682.
36. Keenholtz,R.A., Rowland,S.-J., Boocock,M.R., Stark,W.M. and Rice,P.A. (2011) Structural basis for catalytic activation of a serine recombinase. *Struct. Lond. Engl.*, **19**, 799–809.
37. Yang,W. and Steitz,T.A. (1995) Crystal structure of the site-specific recombinase gamma delta resolvase complexed with a 34 bp cleavage site. *Cell*, **82**, 193–207.
38. Yuan,P., Gupta,K. and Van Duyne,G.D. (2008) Tetrameric structure of a serine integrase catalytic domain. *Struct. Lond. Engl.*, **16**, 1275–1286.
39. Dhar,G., Heiss,J.K. and Johnson,R.C. (2009) Mechanical constraints on Hin subunit rotation imposed by the Fis/enhancer system and DNA supercoiling during site-specific recombination. *Mol. Cell*, **34**, 746–759.
40. Otwinowski,Z. and Minor,W. (1997) Processing of X-ray diffraction data collected in oscillation mode. *Methods Enzymol.*, **276**, 307–326.

41. Strong,M., Sawaya,M.R., Wang,S., Phillips,M., Cascio,D. and Eisenberg,D. (2006) Toward the structural genomics of complexes: crystal structure of a PE/PPE protein complex from Mycobacterium tuberculosis. *Proc. Natl. Acad. Sci. U.S.A.*, **103**, 8060–8065.
42. Adams,P.D., Afonine,P.V., Bunkóczi,G., Chen,V.B., Davis,I.W., Echols,N., Headd,J.J., Hung,L.-W., Kapral,G.J., Grosse-Kunstleve,R.W. *et al.* (2010) PHENIX: a comprehensive Python-based system for macromolecular structure solution. *Acta Crystallogr. D Biol. Crystallogr.*, **66**, 213–221.
43. Haddadian,E.J., Gong,H., Jha,A.K., Yang,X., Debartolo,J., Hinshaw,J.R., Rice,P.A., Sosnick,T.R. and Freed,K.F. (2011) Automated real-space refinement of protein structures using a realistic backbone move set. *Biophys. J.*, **101**, 899–909.
44. Emsley,P. and Cowtan,K. (2004) Coot: model-building tools for molecular graphics. *Acta Crystallogr. D Biol. Crystallogr.*, **60**, 2126–2132.
45. Hubbard,S.J. and Thornton,J.M. (1993) NACCESS Department of Biochemistry and Molecular Biology, University College London.
46. Suhre,K. and Sanejouand,Y.-H. (2004) ElNémo: a normal mode web server for protein movement analysis and the generation of templates for molecular replacement. *Nucleic Acids Res.*, **32**, W610–W614.
47. Keenholtz,R.A., Mouw,K.W., Boocock,M.R., Li,N.-S., Piccirilli,J.A. and Rice,P.A. (2013) Arginine as a general acid catalyst in serine recombinase-mediated DNA cleavage. *J. Biol. Chem.*, **288**, 29206–29214.
48. Krebs,W.G., Alexandrov,V., Wilson,C.A., Echols,N., Yu,H. and Gerstein,M. (2002) Normal mode analysis of macromolecular motions in a database framework: developing mode concentration as a useful classifying statistic. *Proteins*, **48**, 682–695.
49. Delarue,M. and Sanejouand,Y.-H. (2002) Simplified normal mode analysis of conformational transitions in DNA-dependent polymerases: the elastic network model. *J. Mol. Biol.*, **320**, 1011–1024.
50. Tama,F. and Sanejouand,Y.H. (2001) Conformational change of proteins arising from normal mode calculations. *Protein Eng.*, **14**, 1–6.
51. Rice,P.A. (2015) Serine Resolvases. *Microbiol. Spectr.*, **3**, MDNA3–0045–2014.
52. Crick,F.H.C. (1953) The packing of alpha-helices: simple coiled-coils. *Acta Crystallogr.*, **6**, 689–697.
53. Zhang,S.-Q., Kulp,D.W., Schramm,C.A., Mravic,M., Samish,I. and DeGrado,W.F. (2015) The membrane- and soluble-protein helix-helix interactome: similar geometry via different interactions. *Struct. Lond. Engl.*, **23**, 527–541.
54. Chang,Y. and Johnson,R.C. (2015) Controlling tetramer formation, subunit rotation and DNA ligation during Hin-catalyzed DNA inversion. *Nucleic Acids Res.*, **43**, 6459–6472.